Journal of The Electrochemical Society, **157** (10) H964-H968 (2010)
0013-4651/2010/157(10)/H964/5/$28.00 © The Electrochemical Society

$InGaZnO_4$-Based Thin Film Transistors Using Room-Temperature Grown $Mg_2Hf_5O_{12}$ Gate Insulator

Dong Hun Kim,[a] Hyungtak Seo,[b,z] Kwun-Bum Chung,[c] Nam Gyu Cho,[a] Ho-Gi Kim,[a] and Il-Doo Kim[d,z]

[a]*Department of Materials Science and Engineering, Korea Advanced Institute of Science and Technology, Daejeon 305-701, Republic of Korea*
[b]*Materials Sciences Division, Lawrence Berkeley National Laboratory, and Department of Chemistry, University of California, Berkeley, California 94720, USA*
[c]*Department of Physics, Dankook University, Cheonan 330-714, Republic of Korea*
[d]*Optoelectronic Materials Center, Korea Institute of Science and Technology, Cheongryang, Seoul 130-650, Republic of Korea*

This study reports the dielectric and leakage current properties of $Mg_2Hf_5O_{12}$ thin films deposited at room temperature by radio-frequency magnetron sputtering. Polycrystalline $Mg_2Hf_5O_{12}$ thin films showed a reasonably high dielectric constant (ε_r = 22) and greatly enhanced leakage current characteristics ($<2 \times 10^{-7}$ A/cm^2) compared to the leakage current ($\sim 2 \times 10^{-5}$ A/cm^2) of HfO_2 thin films at 0.4 MV/cm. A bandedge spectroscopic analysis revealed lower conduction bandedge defect states and a greater p-type-like Fermi energy level of $Mg_2Hf_5O_{12}$ compared to the HfO_2 thin films. The suitability of $Mg_2Hf_5O_{12}$ films as gate insulators for low voltage operating $InGaZnO_4$ thin film transistors (TFTs) was investigated. All room-temperature processed $InGaZnO_4$ TFTs on plastic substrates exhibited a high field effect mobility of 27.32 cm^2/Vs and a current on/off ratio of 4.01×10^6. The threshold voltage and subthreshold swing were 2 V and 440 mV/dec, respectively. The fabrication and compositional manipulation method of the $Mg_2Hf_5O_{12}$ films described in this work is simple and versatile, providing fascinating opportunities for new high-k gate dielectrics.
 [DOI: 10.1149/1.3465656]

Manuscript submitted February 15, 2010; revised manuscript received June 23, 2010. Published August 25, 2010.

Recently, intensive studies have been carried out on the development of high-k gate insulators suitable for use with flexible and transparent thin film transistors (TFTs). For these types of applications, the gate insulators should be fabricated at a low temperature with high optical transparency. In addition, they should possess a high dielectric constant for lower power consumption in battery-powered devices and other electronic devices.[1-3]

Among various gate insulators, HfO_2 has been widely researched as a high permittivity dielectric oxide for use in thin-film capacitors and TFTs due to its high dielectric constant ($\sim$25), high heat of formation (271 kcal/mol), and large bandgap (5.68 eV).[4-6] Although HfO_2 thin films are one of the prospective candidates for gate insulators, they contain a larger number of trap sites or fixed charges relative to that found in conventional SiO_2 films, resulting in a shift of the threshold voltage, high leakage current, and poor long-term reliability.[7,8] To improve the device properties of TFTs utilizing HfO_2-based gate insulators, silicon, nitrogen, or aluminum-doped HfO_2 thin films have been proposed.[9-12] However, studies of MgO–HfO_2 composite gate insulators that can produce $InGaZnO_4$ TFTs that operate at a low voltage are rare or nonexistent. In a previous work, the authors showed that the leakage current characteristics of $Ba_{0.6}Sr_{0.4}TiO_3$ could be markedly improved by adding MgO, which is a large bandgap insulator with a high breakdown strength.[3] In an effort to improve the dielectric and electrical characteristics of HfO_2 thin films further, in this work, MgO-incorporated HfO_2 films, i.e., novel $Mg_2Hf_5O_{12}$ thin films, are fabricated by radio-frequency (rf) sputtering at room temperature using MgO–HfO_2 composite ceramic targets. The dielectric and leakage current properties of the $Mg_2Hf_5O_{12}$ thin films are characterized and compared with these properties in pure HfO_2 thin films. The physical origin of the differences in the leakage current characteristics between $Mg_2Hf_5O_{12}$ and HfO_2 was identified by the spectroscopically resolved bandedge defect states and the Fermi energy (E_f) levels using spectroscopic ellipsometry (SE) and X-ray photoelectron spectroscopy (XPS). The potential suitability of a $Mg_2Hf_5O_{12}$ thin film as a gate insulator for producing high performance $InGaZnO_4$ TFTs on a plastic substrate is discussed.

[z] E-mail: hseo@lbl.gov; idkim@kist.re.kr

Experimental

HfO_2 and $(MgO)_{0.3}(HfO_2)_{0.7}$ sputtering targets with 2 in. diameters were prepared by a conventional mixed oxide method. To prepare the $(MgO)_{0.3}(HfO_2)_{0.7}$ ceramic targets, a mixture of HfO_2 and MgO powders with a MgO content of 30 mol % was calcined at 1200°C for 3 h. Sintering was conducted at 1400°C under an air atmosphere for 5 h. Details of this fabrication process for an $InGaZnO_4$ target are available in the literature.[3] HfO_2 and $Mg_2Hf_5O_{12}$ thin films were deposited using rf sputtering at an rf power of 80 W and a working pressure of 60 mTorr in a pure Ar atmosphere. The chamber was pumped down to a low base pressure of 10^{-6} Torr. All films were deposited at room temperature without any intentional heating. The film thicknesses of the HfO_2 and $Mg_2Hf_5O_{12}$ thin films were fixed at 300 nm. Structural identification was characterized by an X-ray diffractometer (XRD, Rigaku D/MAX-RC, with Cu Kα radiation, λ = 1.5406 Å). The morphology and microstructure were investigated using a transmission electron microscope (TEM, Tecnai F20) operating at 200 keV. An atomic force microscope (AFM, Seiko, SPA400) was used to investigate the surface roughness of the HfO_2 and $Mg_2Hf_5O_{12}$ thin films. The optical transmittance of 100 nm thick HfO_2 and $Mg_2Hf_5O_{12}$ thin films was measured using a UV-3101 PC spectrophotometer (Shimadzu). The real and imaginary parts of the complex dielectric function, $\varepsilon_c = \varepsilon_1 + i\varepsilon_2$, for the thin films were determined by using visible-UV SE in a rotating compensator configuration spectrometer. XPS was carried out using a VG Scientific Escalab 220i-XL spectrometer with a monochromatic Al Kα radiation source.

A metal–insulator–metal (MIM) capacitor structure was fabricated on a 100 nm thick Pt-coated Si substrate to determine the leakage current and dielectric characteristics of the HfO_2 and $Mg_2Hf_5O_{12}$ thin films. For the top electrode, 100 nm thick Pt was deposited through a shadow mask on top of sputter-deposited HfO_2 and $Mg_2Hf_5O_{12}$ thin films by dc magnetron sputtering. The dielectric properties were measured at 100 kHz with an applied electric field ranging from −0.4 to 0.4 MV/cm using an HP4192A impedance analyzer. An HP4145B semiconductor analyzer was used to measure the leakage current characteristics.

To evaluate the potential suitability of $Mg_2Hf_5O_{12}$ thin films as a gate insulator, $InGaZnO_4$ TFTs were fabricated on a poly(ethylene terephthalate) (PET) substrate. For the fabrication of $InGaZnO_4$

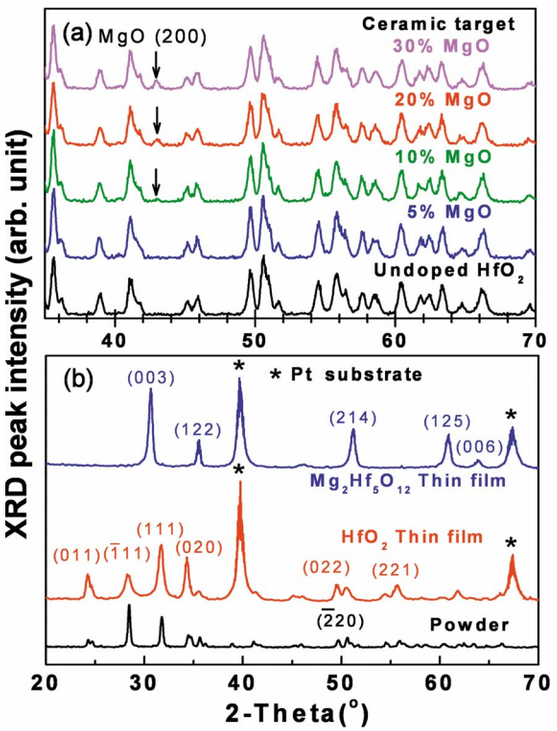

Figure 1. (Color online) XRD patterns of (a) ceramic targets: Undoped, 5, 10, 20, and 30 mol % MgO added HfO_2 ceramic targets sintered at 1400°C. (b) Bare HfO_2 powder or thin films: HfO_2 powder, HfO_2 thin film, and $Mg_2Hf_5O_{12}$ thin film deposited at room temperature on Pt substrates.

TFTs, a 100 nm thick Cr gate electrode was deposited by rf magnetron sputtering on a PET substrate. A sputter-deposited $Mg_2Hf_5O_{12}$ gate insulator and $InGaZnO_4$ channel layer were subsequently grown on the Cr gate electrode. Al top contacts for source and drain electrodes were deposited by evaporation to obtain channel lengths of 100 μm with widths of 2000 μm. For comparison, an $InGaZnO_4$ TFT was also fabricated using pure HfO_2 gate insulators. The performance levels and characteristics measurements of the TFTs were characterized with an HP 4145B semiconductor parameter analyzer.

Results and Discussion

Material characteristics of $Mg_2Hf_5O_{12}$ thin films.— The structural identification of the MgO–HfO_2 composite ceramic targets, HfO_2 powder, HfO_2 thin film, and $(MgO)_{0.3}$–$(HfO_2)_{0.7}$ composite thin film was carried out using XRD, as shown in Fig. 1. Five ceramic targets, consisting of pure MgO, $(MgO)_{0.05}$–$(HfO_2)_{0.95}$, $(MgO)_{0.1}$–$(HfO_2)_{0.9}$, $(MgO)_{0.2}$–$(HfO_2)_{0.8}$, and $(MgO)_{0.3}$–$(HfO_2)_{0.7}$ composites, were fabricated to ascertain the mixing behaviors of MgO with HfO_2. It was concluded that the solubility limit of MgO to HfO_2 ranged from 5 to 10 mol %, as shown in Fig. 1a. The XRD peaks of the 5 mol % MgO–HfO_2 target were identical to those of the HfO_2 target. However, for the HfO_2 composite targets with 10, 20, and 30 mol % of MgO added, the MgO peaks appeared at 43°, while the peaks of HfO_2 were maintained. As the MgO content in the composite targets increased, the intensity of the (200) MgO peak increased, indicating further precipitation of the MgO phases. Based on the scanning electron microscopy (SEM) analysis, the pure HfO_2 target exhibited a homogeneous yellow color. However, the MgO–HfO_2 composite ceramic targets showed two distinct phases uniformly distributed with each other in terms of image contrast. Based on the SEM energy-dispersive X-ray spectroscopy mapping analyses, there were dark regions (MgO-rich) and white regions (HfO_2-rich) (not shown here). The peaks of the HfO_2 target and the HfO_2 thin films were well matched with the monoclinic structure, although the HfO_2 thin film was deposited at room temperature (see Fig. 1b). The structural properties of HfO_2 thin films are largely governed by processing techniques.[13,14] Room-temperature sputtering growth often provides a nanocrystalline structure, whereas HfO_2 films grown by electron-beam evaporation or atomic layer deposition are preferentially amorphous. Figure 1b also shows the XRD pattern of a $(MgO)_{0.3}$–$(HfO_2)_{0.7}$ thin film deposited at room temperature. Similar to HfO_2, the $(MgO)_{0.3}$–$(HfO_2)_{0.7}$ thin film showed a polycrystalline structure, identified as rhombohedral $Mg_2Hf_5O_{12}$ according to JCPDS card no. 33-0862. The XRD peaks of the bulk $(MgO)_{0.3}$–$(HfO_2)_{0.7}$ composite target were wholly different from those of the $Mg_2Hf_5O_{12}$ thin film. This can be attributed to the rearrangement of the Mg^{2+}, Hf^{4+} ions or clusters detached from the $(MgO)_{0.3}$–$(HfO_2)_{0.7}$ composite target, and the formation of a new phase during the sputtering deposition process. To investigate the microstructure of the $Mg_2Hf_5O_{12}$ thin films, high resolution transmission electron microscopy (HRTEM) measurements were carried out.

Figure 2a shows a plane-view TEM image of a $Mg_2Hf_5O_{12}$ thin film deposited at room temperature. This image indicates that $Mg_2Hf_5O_{12}$ thin films grown at room temperature have a polycrystalline structure with a crystallite size distribution of ~20 nm. The average crystallite size was also calculated by the Scherrer equation, $D = (0.94\lambda/B \cdot \cos\theta)$, where D is the mean grain size, λ is the wavelength of the X-ray radiation (λ = 0.154 nm for Cu Kα radiation), and B is the full width at half-maximum of the diffraction peak at θ. This resulted in $D \approx 20$ nm as the average grain size of the $Mg_2Hf_5O_{12}$ thin films. This value agrees with direct measurements obtained using TEM. The selected area electron diffraction pattern of the $Mg_2Hf_5O_{12}$ thin films (upper right inset in Fig. 2a) shows the characteristic diffraction rings, which correspond to reflections (003), (122), (214), and (125) of the rhombohedral structure. The d-spacings calculated from each ring are 2.90, 2.52, 1.78, and 1.52 Å, respectively, as reported in JCPDS card no. 33-0862. Figure 2b shows an HRTEM image of the $Mg_2Hf_5O_{12}$ thin films. The inset in Fig. 2b emphasizes a magnified view of the $Mg_2Hf_5O_{12}$ crystallite. The lattice fringes are clearly visible. In general, a rhombohedral system is grouped into a larger hexagonal system. The interplanar spacings were measured as 2.90, 2.90, and 2.52 Å, corresponding to the (003), (211), and (122) planes of $Mg_2Hf_5O_{12}$. The angle between the (003) and (211) planes was 71° and that between the (003) and (122) planes was 55°. These measured values agree well with the theoretical values, i.e., 70.5 and 54.8°, respectively, for $Mg_2Hf_5O_{12}$. From the phase diagram of the MgO–HfO_2 system,[15] the $Mg_2Hf_5O_{12}$ phase forms at a temperature in excess of 1600°C. This indicates that a very high sintering temperature is required to fabricate a single $Mg_2Hf_5O_{12}$ target from MgO–HfO_2 composites. However, here, it was possible to achieve nanocrystalline $Mg_2Hf_5O_{12}$ thin films utilizing a $(MgO)_{0.3}$–$(HfO_2)_{0.7}$ composite target fabricated at a low sintering temperature of 1400°C.

Dielectric performance and electronic band characteristics of $Mg_2Hf_5O_{12}$ thin films.— Figure 3a shows the dielectric behaviors of HfO_2 and $Mg_2Hf_5O_{12}$ thin films with a thickness of 300 nm as a function of the electric field. The inset in Fig. 3a illustrates a schematic configuration of Pt–HfO_2–Pt and Pt–$Mg_2Hf_5O_{12}$–Pt MIM capacitors. The pure HfO_2 thin film exhibited a relatively high dielectric constant of 23 at 100 kHz. The dielectric constant of the $Mg_2Hf_5O_{12}$ thin film showed a value similar ($\varepsilon_r = 22.5$) to that of HfO_2. Considering the diphasic mixture of the homogeneously distributed individual thin films, i.e., MgO and HfO_2, the dielectric constant should be much lower than 22.5 due to the lower dielectric constant (~9.96) [16] of MgO based on the effective medium approximation using the Bruggerman expression.[17] Assuming a series connection capacitance of the MgO and HfO_2 phases, the dielectric constant should be 16. In this case, MgO combined with HfO_2 and

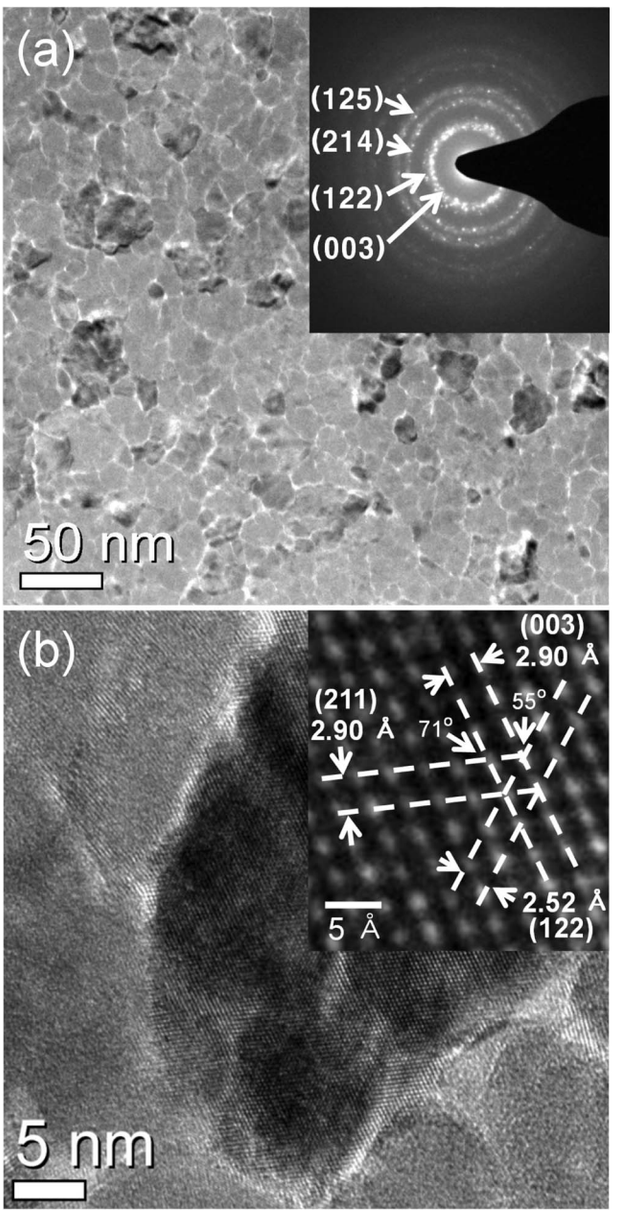

Figure 2. (a) Plane-view of the TEM image of the $Mg_2Hf_5O_{12}$ thin film. The inset is a selected area diffraction pattern of $Mg_2Hf_5O_{12}$ thin film. (b) HR-TEM image of $Mg_2Hf_5O_{12}$ thin film. The inset is a magnified view of $Mg_2Hf_5O_{12}$ crystallite.

formed a single $Mg_2Hf_5O_{12}$ phase, resulting in a high-k value of 22.5. Figure 3b shows the current density of HfO_2 and $Mg_2Hf_5O_{12}$ thin films as a function of the electric field with the configuration of the MIM structure. The HfO_2 thin films exhibited a relatively high leakage current of 2.0×10^{-5} A/cm^2 at 0.3 MV/cm. However, the $Mg_2Hf_5O_{12}$ thin film showed a much lower leakage current of 4.5×10^{-7} A/cm^2 at the same electric field. According to an AFM analysis, the surface morphology was similar (not shown here) and the root-mean-square values of the HfO_2 and $Mg_2Hf_5O_{12}$ thin films were 1.04 and 0.99 nm, respectively. Such a large reduction in the leakage current density is likely not related to the surface morphology but to the material characteristics of $Mg_2Hf_5O_{12}$.

To explain the different J-E (current density-electric field) characteristics in the HfO_2 and $Mg_2Hf_5O_{12}$ thin films, bandedge spectroscopic measurements using SE and XPS were made. These results are shown in Fig. 4a and b. In the imaginary dielectric function (ε_2) spectra shown in Fig. 4a, the ε_2 states above 4.5 eV correspond to the absorption at the conduction band (CB) edge empty states of the HfO_2 and $Mg_2Hf_5O_{12}$ thin films. Below 4.5 eV, both thin films are almost transparent to visible-UV light. Thus, peak states originating from the strained Si surface, which is chemically formed at the Si/dielectric interfaces, are observed at <4.2 eV. The strong absorption onset energy in the ε_2 spectra is usually assigned as the nominal optical bandgap (E_g); these values are 5.67 ± 0.02 and 5.83 ± 0.02 eV for HfO_2 and $Mg_2Hf_5O_{12}$, respectively. Therefore, the optical bandgap of $Mg_2Hf_5O_{12}$ is $\sim 0.16 \pm 0.02$ eV larger than

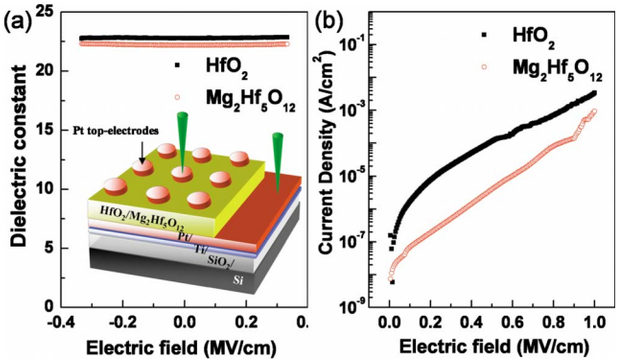

Figure 3. (Color online) (a) The relationship between the dielectric constant and the electric field in HfO_2 and $Mg_2Hf_5O_{12}$ thin films deposited at room temperature. (b) The relationship between the leakage current characteristics and the electric field of HfO_2 and $Mg_2Hf_5O_{12}$ thin films.

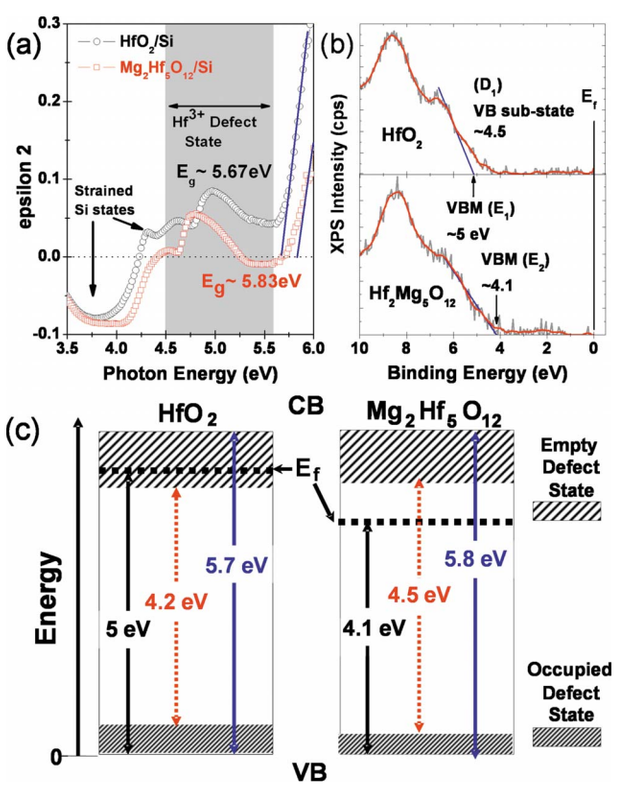

Figure 4. (Color online) (a) Imaginary dielectric function (ε_2) spectra taken from SE measurements: (b) VB edge XPS spectra and (c) schematic bandedge electronic structure model derived from the SE and XPS spectra of HfO_2 and $Mg_2Hf_5O_{12}$.

that of HfO_2. Based on local molecular orbital (MO) theory,[18] the major contribution of the CB onset edge states around the bandgap energy in HfO_2 stems from the empty Hf^{4+} 4d state with e_g bond symmetry mixed with empty O 2p states. This MO state assignment equally holds for the CB onset states in $Mg_2Hf_5O_{12}$ but suggests that the charge transfer between Hf^{4+} 4d and Mg^{2+} 2p states moves the bandgap slightly upward. As the relative density of the Hf 4d states around the bandgap energy is much higher for HfO_2 than $Mg_2Hf_5O_{12}$, a difference in the CB onset state intensity between the two dielectrics is also observed (i.e., a sharp absorption edge at ~5.7 eV in HfO_2 but a weak absorption edge at ~5.8 eV in $Mg_2Hf_5O_{12}$).

More importantly, the significant differences in the CB edge defect state between the two dielectrics are clearly noted. The sub-CB edge states at 4.5–5.5 eV are considered to be empty defect states originating from Hf^{3+} 3d states or oxygen vacancies localized at the grain boundary. This defect state has been commonly observed in the nanocrystalline HfO_2 or Hf silicates.[18] The relative defect density in the ε_2 spectra of HfO_2 is higher than that of $Mg_2Hf_5O_{12}$ over the entire defect state energy range. The charge transport in the nanocrystalline transition-metal oxide including HfO_2 is mainly due to Poole–Frenkel (P–F) hopping and/or trap-assisted tunneling, where pre-existing defects play a major role. Therefore, the lower defect density of $Mg_2Hf_5O_{12}$ in the ε_2 spectra provides the good correlation with the lower leakage current level compared to HfO_2.

As further supporting evidence for the improvement of the leakage current characteristics, the valence band (VB) edge XPS spectra of the HfO_2 and $Mg_2Hf_5O_{12}$ thin films are shown in Fig. 4b. While the double edge states (E_1 and D_1 in Fig. 4b) are resolved in HfO_2, the single edge state (E_2 in Fig. 4b) is resolved in $Mg_2Hf_5O_{12}$. The origin of the double states, E_1 and D_1 in HfO_2, is suggested (*i*) as occupied Hf^{4+} 4d mixed with O 2p MO states assigned as a VB onset edge or a VB maximum edge (E_1) and (ii) as a Hf^{3+} occupied MO state stemming from the same physical origin, an oxygen vacancy having the defect state (D_1) at the CB edge, respectively. The energy position assignment of the VB edge spectra using linearly fitted extrapolation locates the energy level of the D_1 state at ~0.5 eV above the E_1 state. A previous study on VB edge states of HfO_2 thin films resolved by synchrotron soft XPS measurements reports VB edge state features (defect state lying at 0.5 eV above VB onset edge) similar to those in this study.[19] However, discrete VB edge defect states as those in HfO_2 were clearly weaker in the $Mg_2Hf_5O_{12}$. Therefore, the VB edge spectra reinforce the oxygen vacancy defect suppression in $Mg_2Hf_5O_{12}$. In addition, charge transport through the dielectric films at a thickness of ~400 nm in this study is not governed only by a pure tunneling process but by a significant P–F hopping process throughout the bulk oxide. Hence, the E_f position is another crucial reference for bulk charge transport. Following the aforementioned spectral assignments, the E_f levels (0 of binding energy in Fig. 4b) are positioned at 4.6 ± 0.1 eV from the VB onset edge for HfO_2 and at 4.1 ± 0.1 eV for $Mg_2Hf_5O_{12}$. Therefore, the conductivity of the electrons should be lower for $Mg_2Hf_5O_{12}$ than HfO_2. This lower E_f level in $Mg_2Hf_5O_{12}$ also provides the experimentally derived origin of the leakage current suppression.

By combining CB and VB bandedge spectroscopic analyses, a band electronic structure model is proposed, as shown in Fig. 4c. This model, constructed by the experimental results, suggests very plausible origins of the considerable leakage current suppression in $Mg_2Hf_5O_{12}$ thin film. These include (*i*) fewer P–F hopping channels with a lower defect density, (*ii*) a lower CB edge density of state at around the bandgap energy, and (*iii*) a lower E_f level (i.e., more p-type-like and correspondingly lower electron conductivity). The correlation between the structural evolution and observed band structure would be a separate interesting topic, but this future study should include theoretical calculations (e.g., ab initio calculations).

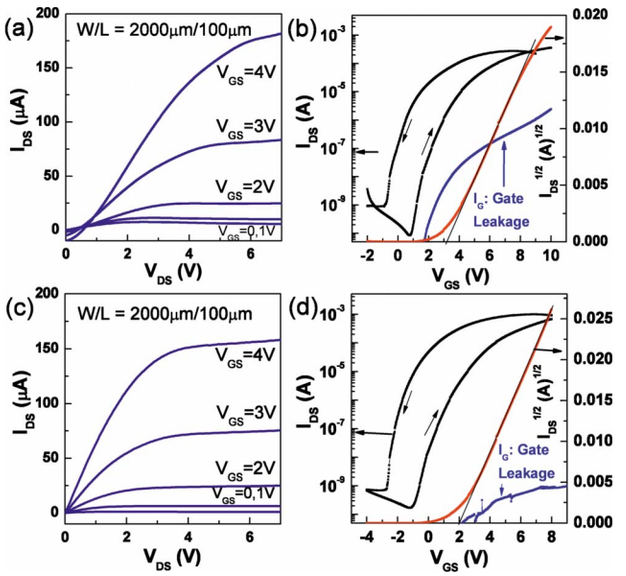

Figure 5. (Color online) (a) The output characteristics of $InGaZnO_4$ TFTs using a HfO_2 gate insulator [a channel length (L) of 100 μm with a channel width (W) of 2000 μm]. (b) The transfer characteristics of $InGaZnO_4$ TFTs using a HfO_2 gate insulator. The voltage between the gate and source was swept from −2 to 10 V at a V_{DS} value of 5 V. (c) The output characteristics of $InGaZnO_4$ TFTs using a $Mg_2Hf_5O_{12}$ gate insulator [a channel length (L) of 100 μm with a channel width (W) of 2000 μm]. (d) The transfer characteristics of $InGaZnO_4$ TFTs using a $Mg_2Hf_5O_{12}$ gate insulator. The voltage between the gate and source was swept from −4 to 8 V at a V_{DS} value of 5 V.

$InGaZnO_4$ TFT performance built on PET substrates using a $Mg_2Hf_5O_{12}$ gate insulator.— Based on structural, physical, and dielectric analyses, $Mg_2Hf_5O_{12}$ thin films are expected to show excellent performance as a gate insulator. Thus, $InGaZnO_4$ TFTs were fabricated using a $Mg_2Hf_5O_{12}$ thin film to demonstrate the suitability of it as a gate insulator on a PET substrate. The same structure of TFTs was compared using a HfO_2 gate insulator. Figure 5a shows the relationship between the drain-to-source current (I_{DS}) and the drain-to-source voltage (V_{DS}) at various gate-to-source voltages (V_{GS}) in $InGaZnO_4$ TFTs using the HfO_2 gate insulator. The value of I_{DS} is nearly 0 at a 0 gate voltage, indicating that TFTs operate in enhancement mode. The TFTs exhibited an on current of 180 μA at a V_{GS} value of 4 V. Moreover, the output characteristics did not exhibit clear current saturation. However, the TFTs using the $Mg_2Hf_5O_{12}$ gate insulator showed good drain-to-source current saturation, as shown in Fig. 5c. The on current was 160 μA at a V_{GS} value of 4 V. The poor saturation characteristics of the TFTs using the HfO_2 gate insulator indicate that free electrons were not entirely depleted at the interface between the $InGaZnO_4$ semiconductor and the HfO_2 gate insulator. Further in-depth study is needed to clarify the correlation between the saturation and interface state. Figure 5b and d shows the transfer characteristics of $InGaZnO_4$ TFTs using HfO_2 and $Mg_2Hf_5O_{12}$ gate insulators with drain-to-source voltages (V_{DS}) of <5 V. The gate voltage was swept from −2 to 10 V for the TFTs using the HfO_2 gate insulator and from −4 to 8 V for the TFTs using the $Mg_2Hf_5O_{12}$ gate insulator. The on current and off current of the TFTs utilizing the HfO_2 gate insulator were 3.59×10^{-4} and 8.41×10^{-11} A, whereas these values for the $Mg_2Hf_5O_{12}$ gate insulator were 6.87×10^{-4} and 1.71×10^{-10} A, respectively, with the on/off current ratios calculated as 4.27×10^6 and 4.01×10^6, respectively. The field effect mobility and threshold voltage were calculated by a linear fit of the $\sqrt{I_{DS}}$ vs V_{GS} curve in the saturation region via the equation $\sqrt{I_{DS}}$

$= \sqrt{(W/2L)C_i\mu}(V_{GS} - V_{TH})$, where C_i is the gate dielectric capacitance per unit area of the gate dielectrics and W and L are the width and length of the channel, respectively. The calculated V_{TH} and μ_{FE} values were 3.2 V and 19.01 cm^2/Vs for the TFTs using the HfO_2 gate insulator, whereas they were 2 V and 27.32 cm^2/Vs, respectively, for the TFTs using the $Mg_2Hf_5O_{12}$ gate insulator. The relation of high-k gate dielectrics to the channel mobility is not due to the higher-k constant of dielectrics but due to the interface quality (e.g., interface traps) between the gate dielectric and channel surface based on the Si-based metal-oxide-semiconductor gate stack research. In the field of oxide TFT, the use of high-k oxides as gate dielectrics commonly exhibits the higher channel mobility than SiO_2. In addition to the better oxide interface quality, another possible mechanism of this phenomenon is the channel mobility dependence of the higher density of field-induced electron density at the channel surface (due to the high capacitance in the accumulation mode). Many papers showed the dependence of bulk or field effect mobility on the intrinsic or field-induced electron concentration in an $InGaZnO_4$ film or channel with high-k gate dielectrics other than SiO_2.[20,21] Therefore, the higher μ_{FE} of TFTs using the $Mg_2Hf_5O_{12}$ gate insulator is ascribed to (*i*) the better interface quality or less oxide traps and (*ii*) the higher density of field-induced electron at the channel surface.

The subthreshold swings were 340 and 440 mV/dec for each TFT. Additionally, there was great improvement in terms of the gate leakage for the TFTs using the $Mg_2Hf_5O_{12}$ gate insulator.

Conclusions

The structural, physical, and dielectric properties of $Mg_2Hf_5O_{12}$ thin film grown at room temperature and its implementation into a flexible $InGaZnO_4$ TFT as a gate insulator were investigated. The $Mg_2Hf_5O_{12}$ thin film showed a high dielectric constant of 22.5 and showed greatly enhanced leakage current characteristics compared to HfO_2 thin film. The reduced defect density and lower E_f level against the VB onset edge in $Mg_2Hf_5O_{12}$ are mainly responsible for the greatly reduced leakage current. $InGaZnO_4$ TFTs with $Mg_2Hf_5O_{12}$ gate insulators exhibited a high field effect mobility of 27.32 cm^2/Vs, a high on/off ratio of 4.01×10^6, and a low threshold voltage of 2 V with a low operating voltage of less than 4 V. These results indicate that $Mg_2Hf_5O_{12}$ thin films show great promise as a high performance gate insulator for the fabrication of highly transparent $InGaZnO_4$ TFTs on plastic substrates.

Acknowledgment

This work was supported by the KIST research program under grant no. 2E21630.

Korea Institute of Science and Technology assisted in meeting the publication costs of this article.

References

1. C. D. Dimitrakopoulos, S. Purushothanman, J. Kymissis, A. Callegari, and J. M. Shaw, *Science*, **283**, 822 (1999).
2. Dhananjay and S. B. Krupanidhi, *J. Appl. Phys.*, **101**, 123717 (2007).
3. D. H. Kim, N. G. Cho, H. G. Kim, H. S. Kim, J. M. Hong, and I. D. Kim, *Appl. Phys. Lett.*, **93**, 032901 (2008).
4. K. Nomura, H. Ohta, K. Ueda, T. Kamiya, M. Hirano, and H. Hosono, *Science*, **300**, 1269 (2003).
5. W. Lim, S. Kim, Y.-L. Wang, J. W. Lee, D. P. Norton, S. J. Pearton, F. Ren, and I. I. Kravchenko, *J. Electrochem. Soc.*, **155**, H383 (2008).
6. J. H. Kim, B. D. Ahn, C. H. Lee, K. A. Jeon, H. S. Kang, and S. Y. Lee, *Thin Solid Films*, **516**, 1529 (2008).
7. T. Tanimura H. Kamada S. Toyoda, H. Kumigashira, M. Oshima, G. L. Liu, Z. Liu, and K. Ikeda, *Appl. Phys. Lett.*, **94**, 082903 (2009).
8. S. Gopalan, K. Onishi, R. Nieh, C. S. Kang, R. Choi, H. J. Cho, S. Crishman, and J. C. Lee, *Appl. Phys. Lett.*, **80**, 4416 (2002).
9. H. B. Park, B. Ju, C. Y. Kang, C. Park, C. S. Park, B. H. Lee, T. W. Kim, B. S. Kim, and R. Choi, *Appl. Phys. Lett.*, **94**, 042911 (2009).
10. S. W. Cho, J. G. Jeong, S. H. Park, M.-H. Cho, K. Jeong, C.-N. Whang, and Y. Yi, *Appl. Phys. Lett.*, **92**, 213302 (2008).
11. R. A. B. Devine, H. N. Alshareef, and M. A. Quevedo-Lopez, *J. Appl. Phys.*, **104**, 124109 (2008).
12. R. Suri, B. Lee, D. J. Lichtenwalner, N. Biswas, and V. Misra, *Appl. Phys. Lett.*, **93**, 193504 (2008).
13. L. Pereira, P. Barquinha, E. Fortunato, R. Martins D. Kang, C. J. Kim, H. Lim, I. Song, and Y. Park, *Thin Solid Films*, **516**, 1544 (2008).
14. H. Hu, C. Zhu, Y. F. Lu, Y. H. Wu, T. Liew M. F. Li, B. J. Cho, W. K. Choi, and N. Yakovlev, *J. Appl. Phys.*, **94**, 551 (2003).
15. K. Wu and Z. Jin, *CALPHAD: Comput. Coupling Phase Diagrams Thermochem.*, **21**, 411 (1997).
16. H. W. Choi, S. Y. Kim, W.-K. Kim, and J.-L. Lee, *Appl. Phys. Lett.*, **87**, 082102 (2005).
17. D. E. Aspnes, *Thin Solid Films*, **89**, 249 (1982).
18. G. Lucovsky, H. Seo, S. Lee, L. B. Fleming, M. D. Ulrich, Jan Lüning, P. Lysaght, and G. Bersuker, *Jpn. J. Appl. Phys., Part 1*, **46**, 1899 (2007).
19. L. Fleming, C. C. Fulton, G. Lucovsky, J. E. Rowe, M. D. Ulrich, and J. Lüning, *J. Appl. Phys.*, **102**, 033707 (2007).
20. Y. W. Choi, I. D. Kim, H. L. Tuller, and A. I. Akinwande, *IEEE Trans. Electron Devices*, **52**, 2819 (2005).
21. C. D. Dimitrakopoulos and P. R. L. Malenfant, *Adv. Mater.*, **14**, 99 (2002).